Early Chromospheric Response During a Solar Microflare Observed With *SOHO*'s CDS and *RHESSI*

Jeffrey W. Brosius

Catholic University of America at NASA Goddard Space Flight Center, Solar Physics Laboratory, Code 671, Greenbelt, MD 20771; Jeffrey.W.Brosius@nasa.gov

Gordon D. Holman

NASA Goddard Space Flight Center, Solar Physics Laboratory, Code 671, Greenbelt, MD 20771; Gordon.D.Holman@nasa.gov

ABSTRACT

We observed a solar microflare with *RHESSI* and *SOHO*'s CDS on 2009 July 5. With CDS we obtained rapid cadence (7 s) stare spectra within a narrow field of view toward the center of AR 11024. The spectra contain emission lines from ions that cover a wide range of temperature, including He I (< 0.025 MK), O V (0.25 MK), Si XII (2 MK), and Fe XIX (8 MK). The start of a precursor burst of He I and O V line emission preceded the steady increase of Fe XIX line emission by about 1 minute, and the emergence of 3-12 keV X-ray emission by about 4 minutes. Thus the onset of the microflare was observed in upper chromospheric (He I) and transition region (O V) line emission before it was detected in high temperature flare plasma emission. Redshifted O V emission during the precursor suggests explosive chromospheric evaporation, but no corresponding blueshifts were found with either Fe XIX (which was very weak) or Si XII. Similarly, in subsequent microflare brightenings the O V and He I intensities increased (between 49 s and almost 2 minutes) before emissions from the hot flare plasma. Although these time differences likely indicate heating by a nonthermal particle beam, the *RHESSI* spectra provide no additional evidence for such a beam. In intervals lasting up to about 3 minutes during several bursts, the He I and O V emission line profiles showed secondary, highly blueshifted (~ -200 km/s) components; during intervals lasting nearly 1 minute the velocities of the primary and secondary components were oppositely directed. Combined with no corresponding blueshifts in either Fe XIX or Si XII, this indicates that explosive chromospheric evaporation occurred predominantly at either comparatively cool temperatures (< 2 MK) or within a hot temperature range to which our observations were not sensitive (*e.g.*, between 2 and 8 MK).

Subject headings: Sun: activity — Sun: corona — Sun: flares — Sun: transition region — Sun: UV radiation — Sun: X-rays, gamma rays

1. Introduction

With its full disk solar imaging capability, wide energy coverage (3 to 17,000 keV), and high sensitivity, the *Ramaty High Energy Solar Spectroscopic Imager* (*RHESSI*; Lin *et al.* 2002; Hurford *et al.* 2002; Smith *et al.* 2002) provides unprecedented capabilities for investigating both nonthermal and high temperature ($\gtrsim 10$ MK) thermal emission from flares and microflares. *RHESSI* has observed more than 25,000 solar microflares (Christe *et al.* 2008) below *GOES* C-class, thus enabling detailed studies of individual events (Krucker *et al.* 2002; Benz & Grigis 2002; Brosius & Holman 2007, 2009; Stoiser *et al.* 2007, 2008; Hannah *et al.* 2008b) as well as a statistical study of the large sample (Hannah *et al.* 2008a). However, *RHESSI* is insensitive to temperatures cooler than about 10 MK, and so provides no direct information about plasma at chromospheric ($T \sim 10^4$ K), transition region ($T \sim 10^5$ K), or coronal ($T \sim 10^6$ K) temperatures. Extreme-ultraviolet (EUV) imagers or spectrometers must be employed to study flare emission at such low temperatures. Further, although *RHESSI* images can be used to measure transverse motions of emitting sources, its spectra cannot be used to measure line-of-sight Doppler velocities; for this one must rely on EUV spectrometers like the Coronal Diagnostic Spectrometer (CDS; Harrison *et al.* 1995) aboard the *SOlar and Heliospheric Observatory* (*SOHO*) spacecraft or the Extreme-ultraviolet Imaging Spectrometer (EIS; Culhane *et al.* 2007) aboard the *Hinode* satellite.

To date comparatively few studies of microflares based on EUV spectra have been reported, largely because the acquisition of spatially resolved spectral data is typically confined to narrow ($1''$ - $4''$), long (hundreds of arcseconds but less than a solar radius) slits. Raster images of a target region are constructed by recording slit spectra at a sequence of pointing positions that cover the desired area. Depending upon the size of the field of view and the number of emission lines selected, the cadences of raster scans range from about 3 to 11 minutes (Czaykowska *et al.* 1999, 2001; Pike & Mason 2002; Teriaca *et al.* 2003, 2006; Falchi *et al.* 2006; Milligan *et al.* 2006a, 2006b; Milligan 2008; Raftery *et al.* 2009). Thus the raster images are not instantaneous, and their time resolutions are longer than the timescales on which flare and microflare emission can vary significantly (Athay *et al.* 1980; Lin *et al.* 1984; Brosius & Phillips 2004; Brosius & Holman 2007, 2009).

The PBEAM observing study was developed to obtain rapid candence (9.8 s) spatially resolved flare spectra with CDS (Brosius 2001, 2003). The study is run in stare mode, and is not used to obtain raster images of its target; coordinated images from *SOHO*'s

Extreme-ultraviolet Imaging Telescope (EIT; Delaboudinière *et al.* 1995) and/or the *Transition Region And Coronal Explorer* (*TRACE*; Handy *et al.* 1999) satellite are almost always available. High time resolution is achieved by recording only selected subsets of the instrument's waveband (549-559 and 590-631 Å, which includes lines formed at temperatures from about 10^5 to 10^7 K), and by compressing spatial information along the $4'' \times 240''$ slit from 143 $4'' \times 1''.68$ pixels to twelve $4'' \times 20''$ pixels. Brosius & Phillips (2004) used this study to investigate the evolution of line intensities and Doppler velocities during a *GOES* M2.3 flare on 2001 April 24. They measured upward (negative) velocities of about -40 km s^{-1} in lines formed at temperatures around 10^5 K during two flare precursors, and concluded that "gentle chromospheric evaporation" (Fisher *et al.* 1985b) occurred at those times. They later measured downward (positive) velocities of about +40 km s^{-1} in the same lines during the flare impulsive phase, when hot ($\sim 10^7$ K) flare lines observed with both CDS (Fe XIX) and the *Yohkoh* satellite's Bragg Crystal Spectrometer (S XV, Ca XIX) became strong and blueshifted, with maximum upward speeds of about -64 km s^{-1}, and concluded that "explosive chromospheric evaporation" (Fisher *et al.* 1985b) occurred during the impulsive phase. The velocities reported by Brosius & Phillips (2004) are consistent with those derived in hydrodynamic simulations by Fisher *et al.* (1985a,b,c), Emslie *et al.* (1992), and Allred *et al.* (2005).

In a process first described but not named by Neupert (1968), "chromospheric evaporation" occurs during flares when energy released by magnetic reconnection in the corona is transported (by nonthermal particle beams and/or thermal conduction) nearly unimpeded to the chromosphere, which is consequently ionized and heated. Nonthermal hard X-ray emission (which *RHESSI* was designed to detect) is produced by the rapid deceleration of beam particles in the chromosphere. When the energy flux into the chromosphere exceeds that which can be shed by radiative losses, the chromosphere heats and expands. Because the overlying coronal density is smaller than the chromospheric and photospheric density, expansion of the heated chromospheric material produces larger upward (negative) velocities than downward (positive) velocities. Upward velocities around -100 km s^{-1} or more seen in emission lines formed at temperatures $\gtrsim 10^7$ K during flares has long been understood as evidence for this phenomenon (Antonucci *et al.* 1982, 1999; Antonucci & Dennis 1983; Zarro *et al.* 1988; Fludra *et al.* 1989; Canfield *et al.* 1990; Doschek 1990; Mariska *et al.* 1993; Mariska 1994; Silva *et al.* 1997; Bornmann 1999; Brosius 2003). Heated, upward-expanding chromospheric material fills loops that appear as hot, dense, thermal flare sources. Evaporation is said to proceed "gently" when Doppler velocities derived with emission lines formed at temperatures characteristic of the upper chromosphere and transition region (as well as hotter lines, if observed) are all directed upward between about -20 and -40 km s^{-1}; evaporation is said to proceed "explosively" when Doppler velocities derived with emission lines formed at

temperatures characteristic of the upper chromosphere and transition region are all directed downward between about 20 and 40 km s^{-1}, while velocities derived from hotter lines are directed upward (Fisher *et al.* 1985b; Brosius & Phillips 2004; Allred *et al.* 2005; Milligan *et al.* 2006a, 2006b; Brosius & Holman 2007, 2009; Brosius 2009). Based on hydrodynamic simulations of a flare loop atmosphere's response to thick-target electron heating, Fisher *et al.* (1985a) found that a beam energy flux around 10^{10} erg cm^{-2} s^{-1} stood as a threshold between gentle and explosive evaporation.

Brosius & Phillips (2004) used the Mg X lines (609.8 and 624.9 Å; formed around 1×10^6 K) in their PBEAM spectra to investigate the behavior of plasma at coronal temperatures. They concluded that both of these lines in flare spectra were likely blended with O IV lines (formed around 1.6×10^5 K), and decided that the unblended line of Si XII at 520.7 Å (formed around 2×10^6 K) would provide a better diagnostic of flare Doppler velocities at coronal temperatures. This led to the development of PBEAM's successor FLAREDOP (Brosius & Holman 2007, 2009; Brosius 2009), which obtains spectra within 515-525, 580-610, and 623-631 Å wavebands. FLAREDOP not only improves observations of flare plasma at coronal temperatures by including Si XII at 520.7 Å, it also extends the temperature range below that available to PBEAM by observing the two upper chromospheric lines of He I (predominantly un-ionized for temperatures $\overset{<}{\sim} 2.5 \times 10^4$ K) at 522.2 and 584.3 Å. Based on intrinsic strength and spectral purity, the four FLAREDOP lines that are most useful for flare and microflare studies include He I at 584.3 Å, O V 629.7 Å (formed at temperatures around 2.5×10^5 K), Si XII 520.7 Å, and Fe XIX 592.2 Å (8×10^6 K).

Brosius & Holman (2007) presented FLAREDOP, EIT, and *RHESSI* observations of a small flare-like transient (FLT) that occurred an arcminute or more away from the flare sources observed with EIT and *RHESSI* during a *GOES* M1.6 flare on 22 July 2004. A brief precursor seen in He I and O V preceded the beginning of the He I and O V impulsive rise by only 20 s. During the impulsive phase, simultaneous, cospatial downward velocities $\approx +30$ km s^{-1} were measured in the He I and O V lines along with upward velocities ≈ -20 km s^{-1} in Si XII and ≈ -150 km s^{-1} in Fe XIX (which remained weak throughout the event), demonstrating that flare-like explosive chromospheric evaporation occurred at this location. A slow increase of Fe XIX emission during the earliest HXR peak in these observations, before any evidence of the FLT was observed in the cool lines, may indicate direct coronal heating prior to the observed precursor and explosive evaporation. Brosius & Holman (2009) presented FLAREDOP and coordinated observations of a *GOES* B2 microflare observed on 16 November 2005. EUV light curves revealed two precursor brightenings, after which the upper chromospheric (He I) and transition region (O V) emission increased for 2.8 minutes before its Fe XIX emission appeared above the noise. Fe XIX emission was evident for only about 2 minutes beginning with the maximum impulsive intensity in the cool EUV lines.

Relative Doppler velocities were directed upward (never downward) with maximum values ≈ -20 km s^{-1} during the second precursor and shortly before the impulsive peak, indicating gentle chromospheric evaporation. The X-ray emission observed by *RHESSI* (up to only 10 keV) revealed no evidence of emission from nonthermal electrons, but did not rule them out.

In order to obtain even better temporal resolution when we observe rapidly varying flare and microflare features like 20 s precursors or rapid impulsive rises, an additional revision to the FLAREDOP study was implemented prior to the observations presented here: the cadence was improved from 9.8 s to about 7.2 s by recording spectral data from only the central 120″ segment of the slit, not its entire 240″ length. The improved cadence, however, is still limited by the readout time. The present work is based on CDS FLAREDOP spectra and coordinated *RHESSI* observations of a *GOES* B1.8 microflare that occurred in AR 11024 on 2009 July 5. We find that (1) increases in the O V and He I intensities consistently preceded increases in hot flare emission (Fe XIX, *RHESSI*, *GOES*); (2) long-lived (up to about 3 minutes) highly blueshifted (-200 km s^{-1}) secondary components were observed in emission line profiles of O V and He I; (3) during intervals lasting nearly 1 minute the velocities of the primary and secondary components were oppositely directed, suggesting explosive chromospheric evaporation. In §2 we describe the observations and data reduction procedures, in §3 we present the results of our analysis, in §4 we discuss implications of our results, and in §5 we summarize our conclusions.

2. Observations and Data Reduction

We observed NOAA Active Region 11024 from 13:34 to 24:00 UT on 2009 July 5 with *SOHO*'s CDS. This was the only active region on the disk at the time. Emission from AR 11024 appeared on the solar east limb on June 29, but the region was not given a number until it was near central meridian on July 4. Only two flares of *GOES* C-class or greater were recorded, including a C2.7 event at 07:07 UT on July 5 and a C1.0 event at 16:59 UT on July 6. Otherwise, the region produced numerous A- and B-class microflares until it rotated behind the limb on July 13. During our observing run *GOES* detected an A-class event that started around 14:30 UT, a B1.4 event that started around 15:42 UT, a B1.8 event that started around 16:30 UT (and was also observed by *RHESSI*), and a B1.0 event that started around 17:34 UT. The B1.8 microflare that was observed by both CDS and *RHESSI* is the subject of the present investigation. In addition to CDS, *RHESSI*, and *GOES* observations, we have full disk Fe XII 195 Å images at 12 minute cadence from *SOHO*'s EIT along with full disk magnetograms from *SOHO*'s Michelson Doppler Imager (MDI; Scherrer *et al.* 1995). *TRACE* was observing quiet Sun area at disk center, and its field of view did not include the

active region. The CME catalog described and maintained by Yashiro *et al.* (2004) indicates no CMEs associated with the microflares observed during this investigation. Throughout this work all spatial positions are expressed in solar disk coordinates (arcsec from disk center) projected to a reference frame at 1 AU (as opposed to *SOHO*'s location at L1).

2.1. EIT and MDI

We acquired a series of full disk Fe XII 195 Å images at 12 minute cadence from EIT, and a full disk synoptic photospheric longitudinal magnetogram (recorded every 96 minutes) from MDI. Figure 1 shows a $4' \times 4'$ magnetogram along with a $4' \times 4'$ 195 Å image of AR 11024 obtained around the time of the microflare. The solid red lines indicate the commanded pointing of the CDS slit, centered around $(119''.8, -458''.2)$; CDS observations (including slit pixels "A" and "B" in which the microflare was observed) are discussed in greater detail below. The actual pointing of CDS is known to differ up to about $10''$ from its commanded value (Thompson 1999a, Brosius 2005), and this uncertainty is overplotted as a dotted red rectangle in Figure 1. Dark areas in the magnetogram represent inward-directed fields (in which the minimum value within the displayed area is -1660 G), and bright areas represent outward-directed fields (in which the maximum value is +1943 G). Note that the microflare brightening that we see in A and B appears to be associated with closely-spaced opposite magnetic polarities a few arcsec east of the slit in Figure 1a.

We found that the image center coordinates from EIT data file headers needed to be reduced by one EIT pixel in each of the x- and y-directions based on a visual inspection algorithm of the limb. The displayed image includes this correction. Under quiescent conditions the EIT 195 Å images are dominated by Fe XII line emission formed around 1.3×10^6 K, but during flares Fe XXIV line emission formed around 2×10^7 K may also contribute. Since, as described below, both *GOES* and *RHESSI* yield thermal plasma temperatures $\sim 1 \times 10^7$ K, we expect little if any Fe XXIV contribution in the EIT images. The overplotted smoothed contours are simply intended to draw attention to the brightest sources in the region. The microflare brightening was altogether unimpressive in the EIT images, and would likely have gone unnoticed had it not been for the *GOES*, *RHESSI*, and CDS observations.

2.2. *RHESSI* and *GOES*

Figure 2 shows the *GOES* 1-8 Å soft X-ray light curve obtained over a five hour interval that includes the four microflares listed above, along with light curves obtained with CDS (see

next subsection) in pixels A and B (see Figure 1). Here we focus on the B1.8 microflare that was observed by *RHESSI* when it was in daylight from about 16:12 to 17:12 UT. A particle event in Earth's magnetosphere contaminated the *RHESSI* light curves with gradual humps that peak toward the center of *RHESSI*'s observing window, but the resulting increased background is not expected to significantly alter the start times or peak times of bursts or brightenings observed during the microflare. Although the B1.8 microflare was the strongest one that occurred during our CDS observing run, *RHESSI* observed it up to energies of only 12 keV. A single, 3-12 keV light curve is shown in Figure 2.

We concentrate particularly on the first half of the microflare, which includes its onset and several impulsive bursts that led up to the plateau of Fe XIX emission seen to start in A around 16:42 UT. In Figure 3 we show a series of *RHESSI* images during the microflare, integrated over 1-minute intervals because the count rates were low. (The total number of counts in each image is between 1×10^4 and 2×10^4.) These images were obtained using the CLEAN technique and *RHESSI* front detectors 3 - 7, giving a spatial resolution $\sim 7''$; images obtained using PIXON (Hurford *et al.* 2002) as well as those including detectors 1 and 9 did not differ significantly from those shown in Figure 3. (Data from detector 8 were contaminated and could not be used.)

The *RHESSI* images in Figure 3 correspond to times before and during two brightenings that occurred within the microflare. The time interval for each image is indicated in the upper right. The CDS slit is overplotted at its commanded pointing centered around $(119''.8, -458''.2)$, with its $10''$ uncertainty overplotted as in Figure 1. Contour levels are the same in all frames, and correspond to 10, 30, 50, and 70% of the maximum count rate in the *RHESSI* image cube. The *RHESSI* images, although on timescales (60 s) coarser than those of the CDS spectra (7.2 s), provide context information for the CDS spectra, and demonstrate that the slit was located in the right place at the right time to obtain EUV spectra of the microflare seen by *GOES* and *RHESSI*. In the analysis that follows we focus on intercomparing light curves from *RHESSI* and *GOES* with light curves and relative Doppler velocities observed with CDS.

The *GOES* and *RHESSI* temperatures at the peak in the *GOES* and *RHESSI* light curves (16:48 UT) were ≈ 10 MK, less than the 12.6 MK median value reported by Hannah *et al.* (2008a) based on a statistical analysis of more than 25,000 microflares observed by *RHESSI*. There was no convincing evidence for a nonthermal component in the *RHESSI* spectra.

2.3. CDS

We employed a new version of the CDS stare study FLAREDOP to obtain EUV spectra at a more rapid cadence ($\sim$ 7.2 s) than was achieved with the older version ($\sim$ 9.8 s). As in the older version, observations within spectral windows of 515-525, 580-610, and 623-631 Å were compressed into $4'' \times 20''$ spatial pixels along the slit, but in the new version of FLAREDOP only the six central such pixels (not all 12) were recorded. This corresponds to a 2-arcmin segment of the 4-arcmin slit, which thus halves the data output and reduces the readout time. See Figure 1.

The commanded pointing of the CDS slit center was $(+119''.8, -458''.2)$ for the entire observing run from 13:33:58 UT until the end of the day on 2009 July 5. During this run we obtained spatially resolved slit spectra in 5250 time intervals. The spectra were processed, calibrated, and analyzed with standard SolarSoftware IDL procedures, including the "broadened Gaussian" line profile fitting procedure developed by Thompson (1999b). Brosius (2003) and Brosius & Phillips (2004) discuss why and how this fitting procedure is used to obtain integrated intensities and centroid wavelengths.

Initially we fit each of the four EUV emission lines on which this investigation is based (He I at 584.3 Å, O V at 629.7 Å, Si XII at 520.7 Å, and Fe XIX at 592.2 Å) with a single broadened Gaussian profile atop a linear background. The resulting integrated line intensities within spatial pixels A and B of the CDS slit (see Figure 1) are displayed as light curves between 14:00 and 19:00 UT in Figure 2. Here the Fe XIX intensity is smoothed with a 9-point running boxcar and plotted on an absolute intensity scale, while the other EUV (and *GOES* and *RHESSI*) light curves are displayed on arbitrary intensity scales. Fe XIX emission is observed only in association with flares and microflares; intensities observed during non-flaring times comprise background noise.

It is well known that solar EUV spectrometers like CDS do not provide rest wavelength scales against which to measure absolute Doppler velocities, but can only be used to measure *relative* Doppler velocities. Thus, the relative Doppler velocity at a particular time and location during an observing run is calculated from the wavelength shift between a "reference" profile centroid (derived within an appropriately designated spatial and temporal interval) and the fitted profile centroid at the desired time and location. Here we select the relatively quiescent period between 15:20 and 15:40 UT, indicated with solid black vertical lines in Figure 2, as our reference interval. This interval is free of microflare activity, as evidenced by the absence of brightenings in the *GOES* and Fe XIX light curves, and is close in time to the start of the B-class microflares. While it is not free of transient brightenings in the He I and O V light curves, none of those brightenings produce particularly large wavelength variations. We derive reference wavelengths (and their associated 1σ scatters) separately for the

lines of He I, O V, and Si XII in each of A and B within this interval by calculating averages (and sigmas) of arrays of profile fit centroids in the sequence of 168 rapid cadence spectra observed during the 20-minute interval. For each of He I, O V, and Si XII we find that their respective reference wavelengths derived separately in pixels A and B agreed within 2 mÅ or less, much better than their associated 1σ scatters (5 and 6 mÅ, respectively, in A and B for He I; 14 and 9 mÅ for O V; and 9 and 7 mÅ for Si XII). Thus, for each of these three emission lines, we combine the fitted centroid wavelength arrays from A and B to derive a single reference wavelength for each ion. For He I, O V, and Si XII the resulting 1σ wavelength scatters correspond to uncertainties in relative Doppler velocity (σ_v) of 3.1, 5.6, and 4.9 km s^{-1}. In what follows we interpret relative Doppler velocities to be significant if they exceed three times the relevant σ_v. Because the Fe XIX emission is essentially just noise in the reference interval, no useful average wavelength can be derived for it.

During a visual inspection of individual line profiles around times of rapid velocity increase, we noticed the emergence of highly blueshifted secondary components. Examples showing a rapid intensity increase of the O V secondary component are given in Figure 4. In order to systematically quantify the presence and properties of such components, we fit each of He I at 584.3 Å, O V at 629.7 Å, and Si XII at 520.7 Å for every exposure in spatial pixels A and B with two broadened Gaussian profiles atop a linear background. The fitting procedure fits two components whether the highly blueshifted secondary component is present or not, but in cases where the secondary component is absent its amplitude is small and its integrated intensity dictated primarily by noise in the spectral background. For fits obtained within the reference interval 15:20 - 15:40 UT, we find that the average ratios of the secondary to primary component intensities are 0.071 ± 0.044 for O V in A and 0.065 ± 0.036 for O V in B; 0.093 ± 0.029 for He I in A and 0.079 ± 0.032 for He I in B; 0.078 ± 0.044 for Si XII in A and 0.076 ± 0.040 for Si XII in B. Figure 5 displays the measured intensity ratios of the secondary to primary components for He I, O V, and Si XII in A and B over a time period that covers the onset and the EUV maxima of the *GOES* B1.8 microflare. Solid horizontal lines indicate 2σ above the average ratios, which values are clearly exceeded by all three spectral lines some of the time in some locations. Indeed, in A the maximum intensity ratio of the secondary component to the primary component exceeds its reference average by 20σ for O V, 15σ for He I, and 3.7σ for Si XII, while in B these values are 29σ for O V, 5.6σ for He I, and no secondary component is found for Si XII. Table 1 lists the time intervals during which these secondary components are found.

For time intervals in which a secondary component is present, the light curves in Figures 6 and 7 (but not Figure 2) show the sum of the two components. Such intervals are displayed in different colors so that they can be readily distinguished. In the relative Doppler velocity plots in Figures 6 and 7 we display the velocities of both components, but reduce that of the

secondary component by a factor of 5 for clarity of display.

3. Results

Figures 6 and 7 (see also Table 2, which gives the times of labeled tick marks in the figures) show normalized light curves of He I, O V, and Fe XIX line emission in CDS pixels A and B, along with the 3-12 keV light curve obtained with *RHESSI*. Here, as in Figure 2, the Fe XIX intensity has been smoothed with a 9-point running boxcar; its average background noise level derived within the reference interval (15:20 - 15:40 UT) is overplotted as a solid green line (slightly different in A than in B), and $\pm 1\sigma$ from this average is overplotted as dotted green lines (also slightly different in A than in B). The light curves show numerous brightenings during the microflare. Here we concentrate on events that led up to and occurred during the earliest 3-12 keV flare brightening (16:30:10 - 16:34:54 UT) as well as three brightenings that occurred immediately thereafter (16:34:54 - 16:38:14, 16:38:14 - 16:39:54, and 16:39:54 - 16:42:26 UT). Except for the start time of the earliest brightening in the above sequence, the start and end times are taken as successive local minima in the 3-12 keV count rate. Peaks or elevated plateaus early in the *GOES* light curve are coincident with those in the *RHESSI* and Fe XIX light curves (see Figure 2), and are not listed here.

3.1. Cool Intensities Increase Before Hot Flare Emission

Both O V and He I participated in what appears to be a precursor burst between about 16:26:00 and 16:28:30 UT. Based on the intensity enhancements involved, the burst is more prominent in A than in B. In A the Fe XIX intensity began to rise steadily from its pre-microflare minimum value at 16:26:46 (the *GOES* emission also rose a bit above its pre-microflare minimum value at this same time) to its average reference value by 16:27:27 UT (after which it stayed above this value), and first exceeded 1σ above this value at 16:28:11 UT. In B the Fe XIX intensity hovered near and below its pre-microflare reference average value until 16:29:14 UT, when it began to increase steadily; it exceeded its reference average intensity by more than 1σ at 16:31:32 (and continued to do so for the duration of the microflare). The earliest start of the 3-12 keV flare emission recorded by *RHESSI* was 16:30:10 UT, about 4 minutes later than the start of the O V precursor burst and more than 3 minutes after the start of the Fe XIX intensity increase in A. Figures 6 and 7 also show that the O V line became significantly redshifted during the precursor burst, with a much more distinct such interval in A (16:26:38 - 16:27:38 UT) than in B ($\sim$ 16:25 - 16:28 UT). The maximum downward speed was only slightly greater in A ($+31$ km s^{-1}) than in

B ($+29$ km s^{-1}). During times surrounding the precursor burst in A the O V emission was generally redshifted ≈ 10 km s^{-1}, while in B it was generally redshifted ≈ 20 km s^{-1}. These downward velocities may be due to cooling, falling material that rained down after having been evaporated upward during the previous B1.4 microflare (see Figure 2). Whatever its origin, the general downflow in B partially masked the velocity signature associated with the (weaker) precursor burst at that location.

The interval of abrupt increase in downward velocity associated with the precursor burst (especially in A) provides evidence for explosive chromospheric evaporation (Fisher *et al.* 1985b; Brosius & Phillips 2004; Brosius & Holman 2007, 2009; Brosius 2009). However, without corroborating measurements of upward velocities in lines formed at higher temperatures, this evidence is inconclusive: the Fe XIX emission is too weak to extract velocity measurements, and Figures 6 and 7 show that velocities measured with Si XII remain near zero. We generated average Fe XIX profiles over selected time intervals (such as the precursor burst and later periods during which upward velocities are expected) in a search for relative Doppler blueshifts, but found none.

The microflare's initial burst of 3-12 keV emission was broad and flat, with a poorly defined maximum around 16:33:20 UT, and ended at 16:34:54 UT, the time of minimum count rate between successive bursts. Similarly, the initial burst of Fe XIX emission in A reached its maximum intensity at 16:33:17 UT (and had a somewhat weaker peak at 16:31:47 UT) and ended at 16:35:26 (the time of its minimum intensity between bursts), while in B it peaked around 16:32:27 and declined gradually after that, reaching a minimum value at 16:36:15 UT, the time at which the next rapid intensity increase (or burst) began. The O V intensity in both A and B decreased to a local minimum value at 16:34:37 UT, after which it increased rapidly before the emergence of highly blueshifted secondary components at 16:35:40 UT in both A and B. See Figures 6 and 7, and Table 2. Thus the O V (and He I) emission shows an impulsive rise at 16:34:37 UT before the hot flare emission in either 3-12 keV (16:34:54 UT, with a more rapid increase beginning at 16:35:30) or Fe XIX (16:35:26 in A, 16:36:15 in B). The fact that emission from the low temperature plasma (He I and O V) increased before that from the high temperature plasma indicates that the chromosphere was involved in the flare before the flare heating mechanism was able to produce a detectable increase in the hot (10 MK) flare emission.

The O V intensity again increased quite rapidly with the re-appearance of secondary, blueshifted components at 16:38:14 UT in both A and B. After that the Fe XIX intensity reached its between-burst minimum value at 16:39:28 UT before starting a rapid increase at this same time in B but not until 16:40:10 in A. The point again is that during this rapid Fe XIX brightening toward its main plateau in A (starting around 16:42 UT) and toward its

greatest intensity in B (16:42:30 UT), the O V intensity increased before that of Fe XIX.

Observations from both *RHESSI* and *GOES* are global while those from CDS are confined to $4'' \times 20''$ pixels A and B. Thus one does not expect to observe an extremely close match between Fe XIX light curves and *RHESSI* or *GOES* light curves. Indeed, the Fe XIX emission provides a more representative signature of the local correspondence between high (Fe XIX) and low (He I and O V) temperature emission than either the 3-12 keV or the 1-8 Å emission. An outstanding example of this is the brightest 3-12 keV peak that occurs between 16:48 and 16:49 UT: *RHESSI* images show that the greatest 3-12 keV brightening at this time was located $20''$ west of the CDS slit, outside its field of view.

The time intervals by which O V emission enhancements precede Fe XIX emission enhancements can be gleaned from Figures 6 and 7 and Table 2, and range from 44 s to about 3 minutes. Specifically, in Figure 6 (location A) we find time differences of 44 s between (a) and (b), 49 s between (d) and (f), and 1 m 56 s between (g) and (h); in Figure 7 (location B) we find time differences of 3 m 5 s between (m) and (n), 1 m 38 s between (d) and (o), and 1 m 14 s between (g) and (p).

3.2. Emergence of Highly Blueshifted Components in Emission Line Profiles

As described above and listed in Table 1, we observed secondary, blueshifted components in each of the He I, O V, and Si XII lines during the microflare. See Figures 4 and 5. The earliest appearance of such components was seen only in O V, and began simultaneously in A and B at 16:35:40 UT. In both locations the O V intensity had begun to increase rapidly starting at 16:34:37 UT before the secondary O V component emerged. In A the Fe XIX intensity began to increase toward its second peak starting at 16:35:26 UT, and in B it began to increase toward its second peak starting at 16:36:15 UT. Thus not only a rapid increase in O V intensity but also the emergence of an O V upward velocity in excess of -200 km s^{-1} is associated with the increase of Fe XIX emission. No significant redshifted emission was observed at this time, indicating that if the rapid upward velocities were due to chromospheric evaporation, such evaporation was gentle (not explosive).

The secondary O V component disappeared for about 1m 44s in A and 43s in B before re-emerging simultaneously in both locations at 16:38:14 UT. The intensity of the secondary component increased steadily until it rivaled that of the primary component; see Figure 4, which shows line profiles in A between 16:38:14 and 16:39:00 UT. Starting from a local minimum at 16:39:28 UT (in both A and B), the Fe XIX intensity steadily increased toward a plateau. This time the secondary component lasted 3m 13s in A, during which He I and Si

XII exhibited blueshifted components of shorter duration than that of O V (see Table 1 and Figure 5). The blueshifted Si XII component endured for only four exposures; during this time the He I and O V lines did not show significant redshifts, so the rapid Si XII upflows were not associated with explosive evaporation.

Late during the lives of the secondary O V components in B we see significant (between $3\sigma_v$ and $7\sigma_v$), sustained (46 s and 55 s) redshifts of the primary component from 16:36:45 to 16:37:31 UT and from 16:39:08 to 16:40:03 UT. See Figure 7 and Table 2. As in other cases where redshifts are observed in chromospheric and transition region emission lines, this suggests explosive evaporation. However, again neither Si XII nor Fe XIX provide evidence for hot, upward flowing material that is needed to corroborate such a conclusion.

3.3. Flare and Microflare EUV Intensity Enhancements

By way of quantifying the EUV emission that we have observed from various types of flares over the years, and to help place the present work's microflare within that context, we give the O V peak intensity (and its enhancement factor compared to the pre-flare average) and the Fe XIX peak intensity (keeping in mind that the Fe XIX emission is essentially non-existent outside of flare times) for previous events. For the *GOES* M6.3 flare of 2001 June 15, Brosius (2003) found a maximum O V intensity of 2.64×10^5 ergs cm^{-2} s^{-1} sr^{-1} (enhancement factor of 270) and a maximum Fe XIX flare intensity of 7.68×10^3 ergs cm^{-2} s^{-1} sr^{-1}. For the *GOES* M2.3 flare of 2001 April 24, Brosius & Phillips (2004) found a maximum O V intensity of 1.41×10^5 ergs cm^{-2} s^{-1} sr^{-1} (enhancement factor of 59) and a maximum Fe XIX flare intensity of 1.26×10^4 ergs cm^{-2} s^{-1} sr^{-1}. For a flare-like transient observed during but spatially separated from a *GOES* M1.6 flare on 2004 July 22, Brosius & Holman (2007) found a maximum O V intensity of about 9×10^3 ergs cm^{-2} s^{-1} sr^{-1} (enhancement factor of 9) and a maximum Fe XIX flare intensity of about 140 ergs cm^{-2} s^{-1} sr^{-1}. For the *GOES* B2 microflare of 2005 November 16, Brosius & Holman (2009) found a maximum O V intensity of about 1.85×10^4 (enhancement factor of about 11; see their Figure 4) and a maximum Fe XIX flare intensity of about 260 ergs cm^{-2} s^{-1} sr^{-1}. For the *GOES* M1.5 flare of 2004 July 27, Brosius (2009) observed a maximum O V intensity of about 4.4×10^4 (enhancement factor of about 7; see his Figure 5, lower segment) and a maximum Fe XIX intensity of 1.26×10^4 (see his Figure 3, middle segment). This flare occurred in a flare-productive active region, and the "starting" intensities for all the lines appear to have been elevated due to earlier flare activity.

For the B1.8 microflare under present investigation we find maximum O V intensities of 3.35×10^4 ergs cm^{-2} s^{-1} sr^{-1} in A and 1.95×10^4 in B, both of which are sums of the

main and secondary, blueshifted components observed in the line profiles. Compared to the pre-microflare reference intensities of 4.45×10^3 in A and 3.97×10^3 in B, the maxima correspond to intensity enhancement factors of 7.53 and 4.91. These enhancement factors, as well as the maximum Fe XIX intensities of only about 100 ergs cm^{-2} s^{-1} sr^{-1} in both A and B (see Figure 2), are consistent with those measured during previous microflares.

4. Discussion

The fact that a "precursor" burst of upper chromospheric (He I) and transition region (O V) EUV emission occurred in the same place and began only four minutes earlier than the *GOES* B1.8 microflare strongly suggests that the precursor and the microflare were related. Indeed the slow steady increase of Fe XIX intensity in A during the precursor supports this suggestion. However, we cannot rule out the possibility that the EUV precursor is instead an independent transient phenomenon that just happened to be in the right place at nearly the right time. Figures 6 and 7 show that the Fe XIX emission remained extremely weak, and did not continuously exceed its reference average by more than 1σ in either A or B until after the precursor had ended.

However if, as we expect, the EUV precursor is associated with the microflare, it indicates that the chromosphere was involved before hot flare plasma was present, which strongly suggests that the dominant energy transport mechanism early during the flare was an electron beam, not thermal conduction from a reconnection-heated hot coronal source. If the EUV precursor were due to thermal conduction, then *GOES* or *RHESSI* should have seen hot (~ 10 MK) flare emission before CDS recorded intensity enhancements in much cooler plasma (0.025 to 0.25 MK). It could perhaps be argued that the emission measure of the ~ 10 MK flare plasma was so small that it was invisible to *GOES* or *RHESSI*, but in that case the energy available in the hot coronal flare source would likely be insufficient to conductively ionize and heat the chromosphere and eventually drive upflows to more than -200 km s^{-1}. It is possible that the redshifted O V emission during the precursor indicates explosive chromospheric evaporation, but without observations of simultaneous upward velocities in any other emission lines this cannot be demonstrated conclusively. The *RHESSI* spectra, because of the low count rate relative to the background count rate, were of low quality and could not provide additional evidence for a nonthermal component and, therefore, an electron beam.

The key for identifying explosive chromospheric evaporation with EUV spectroscopy is to observe simultaneous, cospatial (at least, within the same pixel which in our case covers a $4'' \times 20''$ area) upward velocities in hot flare emission (Fe XIX, maybe Si XII), and downward

velocities in transition region (He II, O III, O V) and upper chromospheric (He I) emission. Similarly, in the case of gentle evaporation, all velocities would be directed upward. If the redshifted O V emission during the precursor indicates explosive evaporation, then the absence of observed simultaneous upward velocities in either Si XII or Fe XIX means that the upward velocities occurred predominantly at temperatures between those of O V and Si XII (0.25-2 MK) or between those of Si XII and Fe XIX (2-8 MK), or perhaps even at temperatures greater that that of Fe XIX (> 8 MK). If the upward velocities occurred predominantly at temperatures between 0.25 MK and 2 MK, the explosive evaporation might be said to have been "cold." (Cold explosive chromospheric evaporation seems to be what we observed during the 46 s and 55 s intervals in which the O V line profiles showed simultaneous upward velocities approaching -200 km s^{-1} and downward velocities approaching 40 km s^{-1}). If the explosive chromospheric evaporation were cold, then the microflare's particle beam was insufficient to heat the chromosphere to $\sim$ 10 MK flare temperatures, in which case the Fe XIX emission and thermal flare emission observed by *RHESSI* were produced by direct heating in the corona. If the upward velocities occurred predominantly at temperatures between 2 MK and 8 MK (or at temperatures in excess of 8 MK), then it would have occurred at temperatures in excess of average coronal temperatures, and might be thought to have been "hot" or "standard" explosive chromospheric evaporation. This would be worth pursuing with coordinated CDS and EIS observations in order to achieve more extensive temperature coverage. It will also be useful to coordinate these types of rapid cadence spectroscopic observations with rapid cadence multiwaveband imagery from the Atmospheric Imaging Assembly (AIA) aboard the *Solar Dynamics Observatory (SDO)*.

In intervals lasting up to about 3 minutes during several bursts, the He I and O V emission line profiles showed secondary, highly blueshifted (~ -200 km/s) components; during intervals lasting nearly 1 minute the velocities of the primary and secondary components were oppositely directed, a signature of explosive chromospheric evaporation. No corresponding blueshifts were found in either Fe XIX (based on profiles averaged over selected exposures) or Si XII, which means that the explosive evaporation was either "cold" (confined to temperatures less than 2 MK) or occurred predominantly in a hot temperature range to which our observations were not sensitive (perhaps somewhere between 2 and 8 MK).

The Si XII brief (4 exposures) interval of secondary blueshifted emission occurred only in A, and at a time when the O V main component was slightly (but not significantly) blueshifted. In any case no redshift was observed during the brief interval of blueshifted Si XII emission, ruling out explosive evaporation at that time.

Based on a sample calculation using their EBTEL model for loop strand heating by nanoflares, Klimchuk *et al.* (2008) found that the temperature at the coronal energy release

site was smaller when a portion of the released energy was used to accelerate an electron beam than it was when no electron beam was produced (see their Fig. 8). Thus their model calculation supports our contention that an electron beam heated the chromosphere and drove evaporation during our microflare, and no hot flare source was observed until after chromospheric and transition region emission had begun to increase.

Berkebile-Stoiser *et al.* (2009) present extensive observations of a series of three *GOES* A-class microflares that include CDS stare spectra at 15 s cadence in lines of He I, O V, and Si XII. Rest wavelengths were derived from averaged quiet portions of narrow raster images. They found that the CDS profiles of several lines show two or three components during 1 to 3 exposures in several different locations around the microflares' peaks, and interpret these oppositely directed velocities in terms of twisting motion of the flare loop. A key difference between their observations and ours is that they find larger downward (+180 km s^{-1}) than upward (-80 km s^{-1}) velocities, while we find larger upward (around -200 km s^{-1}) than downward (+40 km s^{-1}) velocities.

The B1.4 microflare that started around 15:42 UT and the B1.8 microflare under present investigation appear as distinct events in the *GOES* and Fe XIX light curves, but appear blended and inseparable (almost like one continuous event) in the Si XII, O V, and He I emission. The blended appearance of the microflare light curves is more apparent in A than in B (see Figure 2). This is qualitatively similar to what is expected in the nanoflare heating model of the solar corona, in which a sporadic succession of localized, transient heating to super-coronal temperatures become indistinguishable when they cool to representative coronal temperatures around 2×10^6 K.

5. Summary

We have presented CDS and *RHESSI* observations of a B1.8 microflare. With CDS we obtained rapid cadence (7 s) EUV stare spectra that contain emission lines from ions formed over a wide range of temperature, including He I at 584.3 Å (< 0.025 MK), O V 629.7 Å (0.25 MK), Si XII 520.7 Å (2 MK), and Fe XIX 592.2 Å (8 MK). The start of a precursor burst of He I and O V line emission preceded the steady increase of Fe XIX line emission by about 1 minute, and the emergence of 3-12 keV X-ray emission by about 4 minutes. Thus the onset of the microflare was observed in upper chromospheric (He I) and transition region (O V) line emission before it was detected in high temperature flare plasma emission. Redshifted O V emission during the precursor suggests explosive chromospheric evaporation, but this could not be confirmed because no corresponding blueshifts were found with either Fe XIX (which was very weak) or Si XII. Similarly, in subsequent microflare brightenings the O V

and He I intensities increased (between 49 s and almost 2 minutes) before emissions from the hot flare plasma. These time differences likely indicate heating by a nonthermal particle beam during the microflare. Unfortunately, because of their low quality, the *RHESSI* spectra provide no additional evidence for such a beam. In intervals lasting up to about 3 minutes during several bursts, the He I and O V emission line profiles showed secondary, highly blueshifted (~ -200 km/s) components whose intensities sometimes rivaled those of the primary component. During intervals lasting nearly 1 minute the velocities of the primary and secondary components were oppositely directed. Combined with no corresponding blueshifts in either Fe XIX or Si XII, this indicates that explosive chromospheric evaporation occurred predominantly at either comparatively cool temperatures (< 2 MK) or within a hot temperature range to which our observations were not sensitive (*e.g.*, between 2 and 8 MK).

REFERENCES

Allred, J. C., Hawley, S. L., Abbett, W. P., & Carlsson, M. 2005, ApJ, 630, 573

Antonucci, E., Alexander, D., Culhane, J. L., de Jager, C., MacNeice, P., Somov, B. V., & Zarro, D. M. 1999, in The Many Faces of the Sun, ed. K. T. Strong, J. L. R. Saba, B. M. Haisch, & J. T. Schmelz (New York: Springer), p. 331

Antonucci, E., & Dennis, B. R. 1983, Sol. Phys., 86, 67

Antonucci, E., *et al.* 1982, Sol. Phys., 78, 107

Athay, R. G., White, O. R., Lites, B. W., & Bruner, E. C., Jr. 1980, Sol. Phys., 66, 357

Benz, A. O., & Grigis, P. C. 2002, Sol. Phys., 210, 431

Berkebile-Stoiser, S., Gomory, P., Veronig, A. M., Rybak, J., & Sutterlin, P. 2009, A&A, 505, 811

Bornmann, P. L. 1999, in The Many Faces of the Sun, ed. K. T. Strong, J. L. R. Saba, B. M. Haisch, & J. T. Schmelz (New York: Springer), p. 301

Brosius, J. W. 2001, ApJ, 555, 435

Brosius, J. W. 2003, ApJ, 586, 1417

Brosius, J. W. 2005, ApJ, 622, 1216

Brosius, J. W. 2009, ApJ, 701, 1209

Brosius, J. W., & Holman, G. D. 2007, ApJ, 659, L73

Brosius, J. W., & Holman, G. D. 2009, ApJ, 692, 492

Brosius, J. W., & Phillips, K. J. H. 2004, ApJ, 613, 580

Canfield, R. C., Zarro, D. M., Metcalf, T. R., & Lemen, J. R. 1990, ApJ, 348, 333

Christe, S., Hannah, I. G., Krucker, S., McTiernan, J., & Lin, R. P. 2008, ApJ, 677, 1385

Culhane, J. L., *et al.* 2007, Sol. Phys., 243, 19

Czaykowska, A., Alexander, D., & De Pontieu, B. 2001, ApJ, 552, 849

Czaykowska, A., De Pontieu, B., Alexander, D., & Rank, G. 1999, ApJ, 521, L75

Delaboudinière, J.-P., *et al.* 1995, Sol. Phys., 162, 291

Doschek, G. A. 1990, ApJS, 73, 117

Emslie, A. G., Li, P., & Mariska, J. T. 1992, ApJ, 399, 714

Falchi, A., Teriaca, L., & Maltagliati, L. 2006, Sol. Phys., 239, 193

Fisher, G. H., Canfield, R. C., & McClymont, A. N. 1985a, ApJ, 289, 414

Fisher, G. H., Canfield, R. C., & McClymont, A. N. 1985b, ApJ, 289, 425

Fisher, G. H., Canfield, R. C., & McClymont, A. N. 1985c, ApJ, 289, 434

Fludra, A., Lemen, J. R., Jakimiec, J., Bentley, R. D., & Sylwester, J. 1989, ApJ, 344, 991

Handy, B. N., *et al.* 1999, Sol. Phys., 187, 229

Hannah, I. G., Christe, S., Krucker, S., Hurford, G. J., Hudson, H. S., & Lin, R. P. 2008a, ApJ, 677, 704

Hannah, I. G., Krucker, S., Hudson, H. S., Christe, S., & Lin, R. P. 2008b, A&A, 481, L45

Harrison, R. A., *et al.* 1995, Sol. Phys., 162, 233

Hurford, G. J., Schmahl, E. J., Schwartz, R. A., *et al.* 2002, Sol. Phys., 210, 61

Klimchuk, J. A., Patsourakos, S., & Cargill, P. J. 2008, ApJ, 682, 1351

Krucker, S., Christe, S., Lin, R. P., Hurford, G. J., & Schwartz, R. A. 2002, Sol. Phys., 210, 445

Lin, R. P., *et al.* 2002, Sol. Phys., 210, 3

Lin, R. P., Schwartz, R. A., Kane, S. R., Pelling, R. M., & Hurley, K. C. 1984, ApJ, 283, 421

Mariska, J. T. 1994, ApJ, 434, 756

Mariska, J. T., Doschek, G. A., & Bentley, R. D. 1993, ApJ, 419, 418

Milligan, R. O. 2008, ApJ, 680, L157

Milligan, R. O., Gallagher, P. T., Mathioudakis, M., Bloomfield, D. S., Keenan, F. P., & Schwartz, R. A. 2006a, ApJ, 638, L117

Milligan, R. O., Gallagher, P. T., Mathioudakis, M., & Keenan, F. P. 2006b, ApJ, 642, L169

Neupert, W. M. 1968, ApJ, 153, L59

Pike, C. D., & Mason, H. E. 2002, Sol. Phys., 206, 359

Raftery, C. L., Gallagher, P. T., Milligan, R. O., & Klimchuk, J. A. 2009, A&AS, 494, 1127

Scherrer, P. H., *et al.* 1995, Sol. Phys., 162, 129

Silva, A. V. R., Wang, H., Gary, D. E., Nitta, N., & Zirin, H. 1997, ApJ, 481, 978

Smith, D. M., *et al.* 2002, Sol. Phys., 210, 33

Stoiser, S., Brown, J. C., & Veronig, A. M. 2008, Sol. Phys., 250, 315

Stoiser, S., Veronig, A. M., Aurass, H., & Hanslmeier, A. 2007, Sol. Phys., 246, 339

Teriaca, L., Falchi, A., Cauzzi, G., Falciani, R., Smaldone, L. A., & Andretta, V. 2003, ApJ, 588, 596

Teriaca, L., Falchi, A., Falciani, R., Cauzzi, G., & Maltagliati, L. 2006, A&A, 455, 1123

Thompson, W. T. 1999a, CDS Software Note 48,
    http://solar.bnsc.rl.ac.uk/swnotes/cds_swnote_48.pdf

Thompson, W. T. 1999b, CDS Software Note 53,
    http://solar.bnsc.rl.ac.uk/swnotes/cds_swnote_53.pdf

Yashiro, S., Gopalswamy, N., Michalek, G., St. Cyr, O. C., Plunkett, S. P., Rich, N. B., &
    Howard, R. A. 2004, J. Geophys. Res., 109, A07105

Zarro, D. M., Canfield, R. C., Strong, K. T., & Metcalf, T. R. 1988, ApJ, 324, 582

Table 1. Times (UT) of Significant, Blueshifted Emission Line Components.

Emission Line	Source "A"	Source "B"
He I 584.3 Å	16:38:21 - 16:40:18	16:38:14 - 16:39:08
O V 629.7 Å	16:35:40 - 16:36:30	16:35:40 - 16:37:31
	16:38:14 - 16:41:27	16:38:14 - 16:40:03
	$\cdots$	16:49:39 - 16:53:02
Si XII 520.7 Å	16:38:37 - 16:39:01	$\cdots$

Table 2. Times (UT) of Selected Events.

Event	Source "A"	Source "B"
Start O V and He I precursor burst	16:26:02 (a)	16:26:09 (m)
Start O V 3σ redshift	16:26:38 (i)	$\sim$ 16:25
End O V 3σ redshift	16:27:38 (j)	$\sim$ 16:28
Start Fe XIX intensity increase	16:26:46 (b)	16:29:14 (n)
Fe XIX first exceeds $I_0 + 1\sigma$	16:28:11	16:31:32
Fe XIX stays above $I_0 + 1\sigma$	16:29:58	16:31:32
Earliest start of 3-12 keV emission	16:30:10 (c)	16:30:10 (c)
Earliest start of 1-8 Å emission	16:30:39	16:30:39
Start rapid O V intensity increase	16:34:37 (d)	16:34:37 (d)
Start O V 3σ redshift	16:34:52 (k)	16:34:45 (q)
3-12 keV between-burst minimum	16:34:54 (e)	16:34:54 (e)
End O V 3σ redshift	16:35:26 (L)	16:35:33 (r)
Fe XIX between-burst minimum	16:35:26 (f)	16:36:15 (o)
Start blueshifted O V component	16:35:40	16:35:40
Start 3-12 keV brightening	16:35:42	16:35:42
Start redshifted O V main component	$\cdots$	16:36:45 (s)
End redshifted O V main component	$\cdots$	16:37:31 (t)
End blueshifted O V component	16:36:30	16:37:31
A peak in the 3-12 keV emission	16:37:06	16:37:06
Resume blueshifted O V component	16:38:14 (g)	16:38:14 (g)
Start rapid O V intensity increase	16:38:14 (g)	16:38:14 (g)
Start 3-12 keV brightening	16:38:14	16:38:14
Start redshifted O V main component	$\cdots$	16:39:08 (u)
A peak in the 3-12 keV emission	16:39:10	16:39:10
Fe XIX between-peak minimum	16:39:28 (p)	16:39:28 (p)
Start 3-12 keV brightening	16:39:54	16:39:54
Maximum O V intensity	16:39:56	16:38:37
Fe XIX intensity rise to main plateau	16:40:10 (h)	16:39:28 (p)
End redshifted O V main component	$\cdots$	16:40:03 (v)
A peak in the 3-12 keV emission	16:40:58	16:40:58
End blueshifted O V component	16:41:27	16:40:03

Note. — Event times labeled with a letter (in parentheses) are indicated with the same letter in Figures 6 and 7. The letter labels are arranged alphabetically in the figures, but are out of order in the list above.
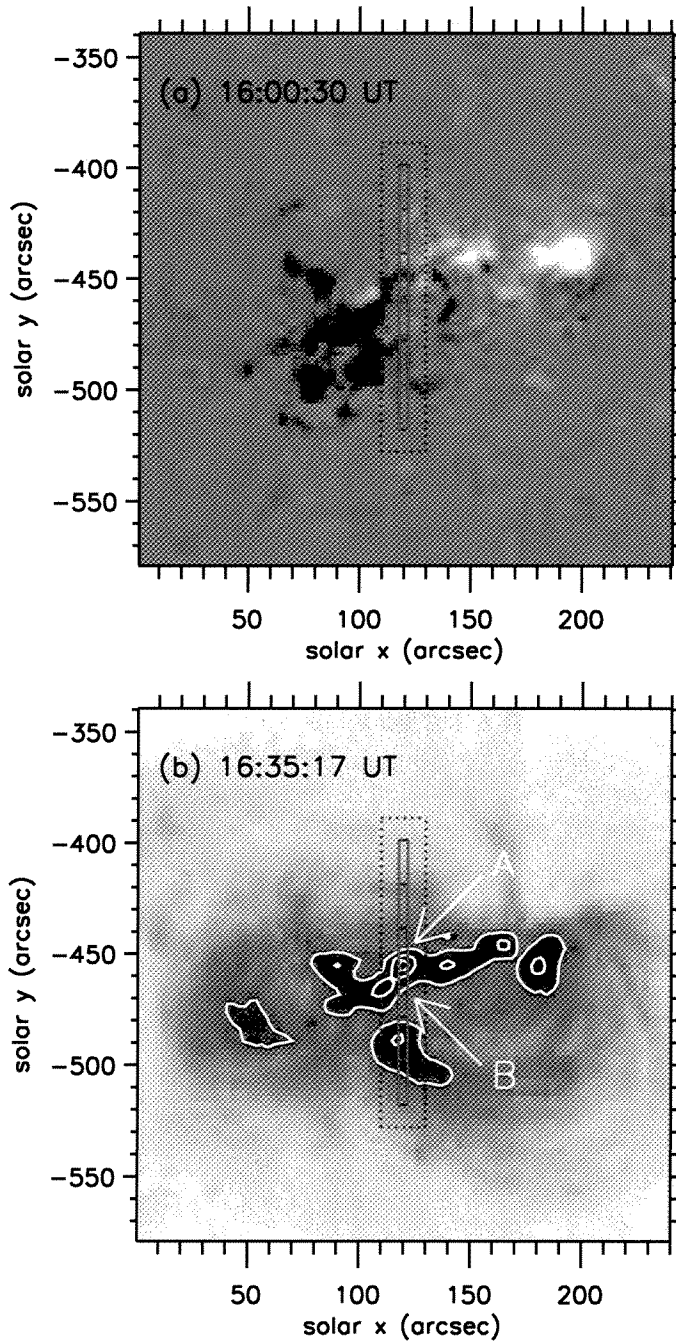
Fig. 1.— A $4' \times 4'$ MDI photospheric longitudinal magnetogram (a), and a $4' \times 4'$ EIT Fe XII 195 Å image (b) obtained at the times indicated in each frame on 2009 July 5. The position of the CDS slit is outlined in red as six $4'' \times 20''$ segments into which its spatially resolved spectra were binned, centered around its commanded pointing at $(119''.8, -458''.2)$. The $\sim 10''$ uncertainty in the CDS pointing (see text) is overplotted as a dotted red rectangle. Slit pixels "A" and "B" in which the microflare was observed with CDS are indicated in (b). All angular measurements are referenced to 1 AU (as opposed to *SOHO*'s location at L1).
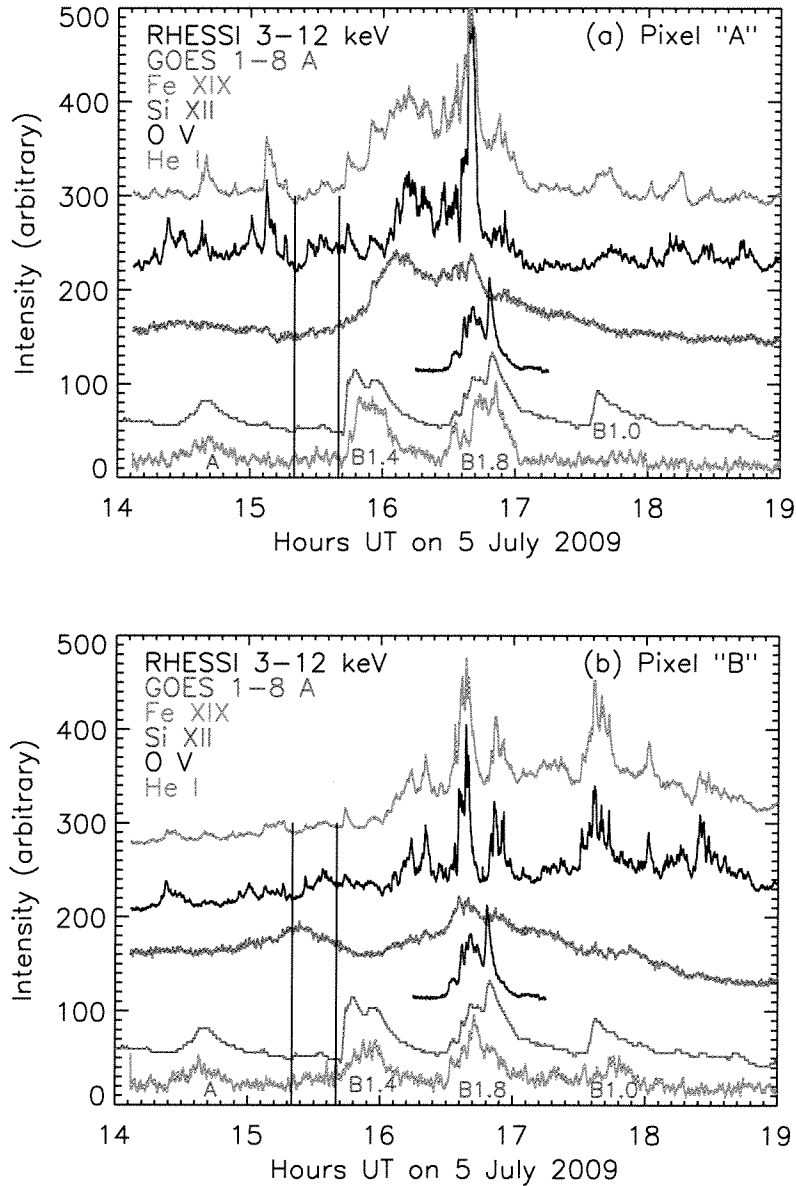
Fig. 2.— EUV light curves of He I, O V, Si XII, and Fe XIX from CDS in (a) pixel A and (b) pixel B (see Figure 1), along with the 1-8 Å soft X-ray light curve from *GOES* and the 3-12 keV light curve from *RHESSI*. The Fe XIX intensity in both frames has been smoothed with a 9-point running boxcar, and is plotted on an absolute intensity scale; all other light curves are plotted on arbitrary (but the same in both frames) scales for ease of inter-comparison. The solid vertical lines near the beginning of both frames indicate a relatively quiescent interval (15:20-15:40 UT) from which various "reference" quantities (including wavelengths common to both frames; see text) are derived.
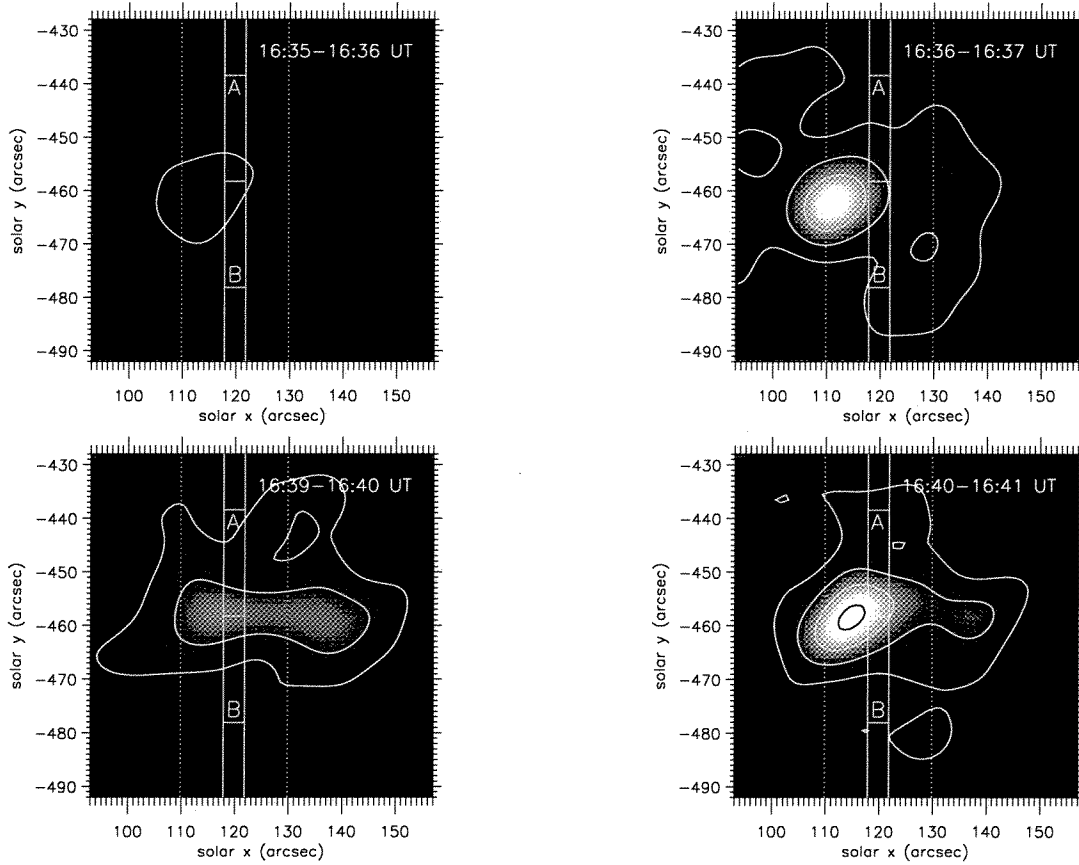
Fig. 3.— A series of *RHESSI* 3-12 keV 1-minute images showing two successive bursts or brightenings during the microflare. These images were obtained using the CLEAN technique and *RHESSI* front detectors 3 - 7, giving a spatial resolution $\sim 7''$. The time interval for each image is indicated in the upper right. "Before" frames are in the left column, and "during" frames are in the right. The CDS slit is overplotted at its commanded center pointing of $(119''.8, -458''.2)$, with an uncertainty of $10''$ as discussed in the text. Contour levels are the same in all frames, and correspond to 10, 30, 50, and 70% of the maximum count rate in the *RHESSI* image cube. The highest contour is displayed in black so that it is visible within the bright flare source. All images are displayed on the same brightness scale.
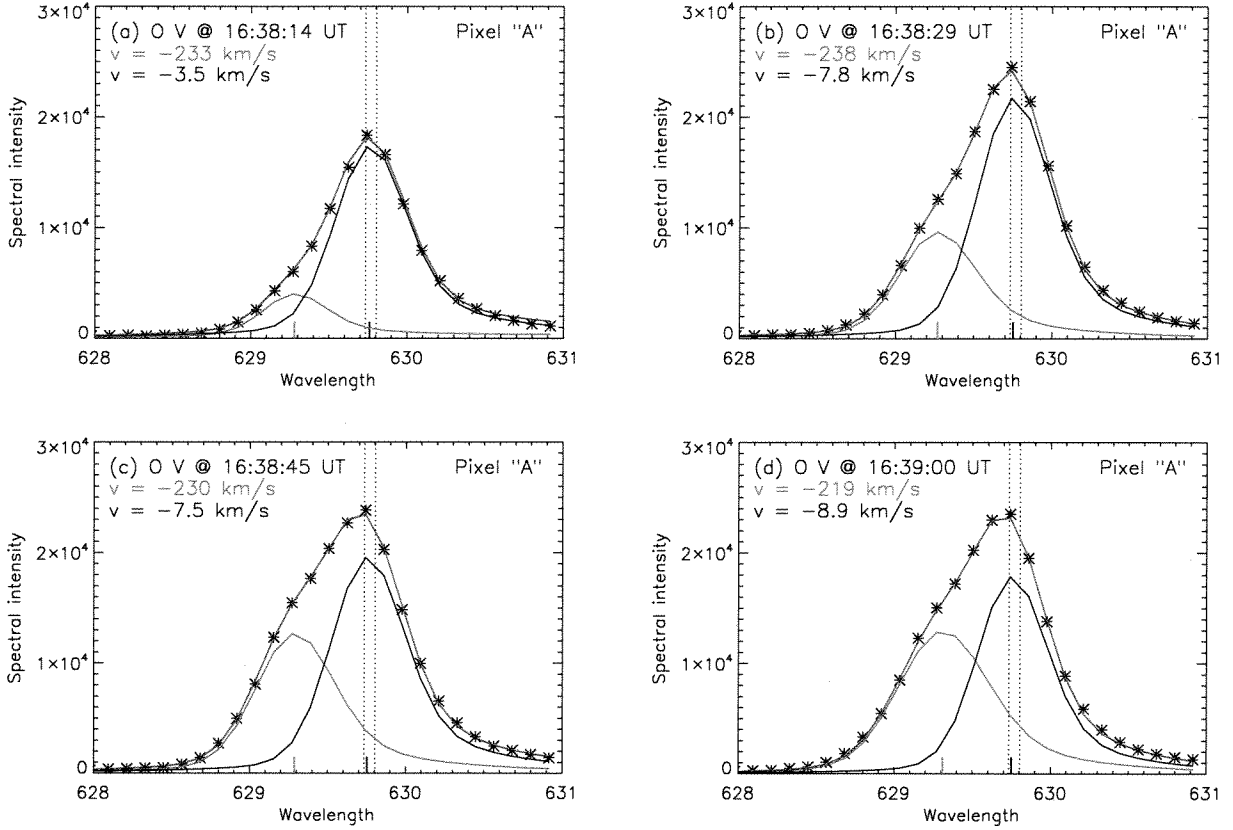
Fig. 4.— Sequence of O V 629.7 Å profiles (spectral intensity in ergs cm^{-2} s^{-1} sr^{-1} Å^{-1} *vs.* wavelength in Å) showing the rapid rise of the secondary blueshifted component from 16:38:14 to 16:39:00 UT in location "A". The central time of each exposure is indicated in the upper left of each frame, and there is one additional exposure (not shown here) between each frame. The observed profile is displayed as black asterisks, the "main" and "blueshifted" components are displayed as solid black and blue curves, respectively, and the net fitted profile is displayed as a solid red curve. Dotted vertical lines indicate $\pm 3\sigma$ from the reference wavelength (see text). Short solid black and blue vertical lines indicate the centroid wavelengths of the main and blueshifted components, the corresponding velocities of which are given in the upper left of each frame.
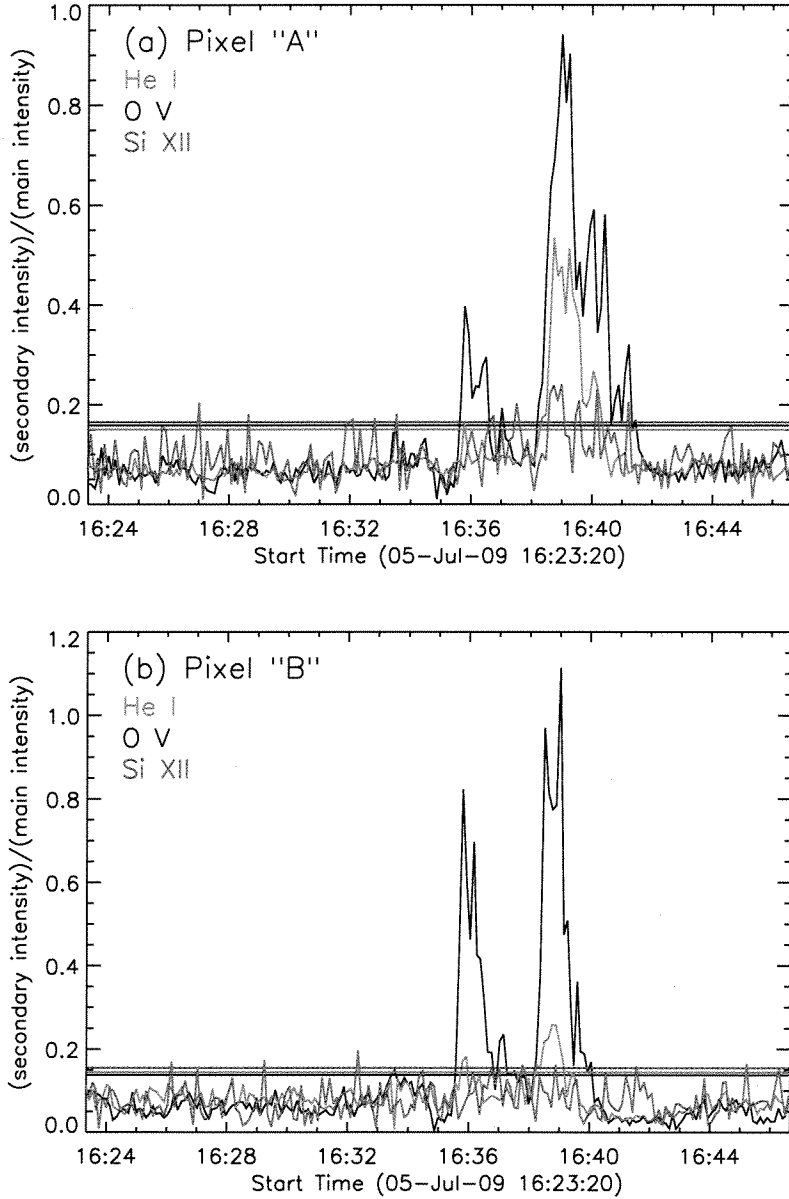
Fig. 5.— Intensity ratio of the secondary, blueshifted component to the main component for O V, He I, and Si XII in (a) pixel "A" and (b) pixel "B". Horizontal lines indicate 2σ above the average ratios derived in the relatively quiescent "reference" interval (15:20-15:40 UT) during which the secondary component is considered to be noise. Time intervals in which we find significant, secondary, blueshifted components are listed in Table 1.
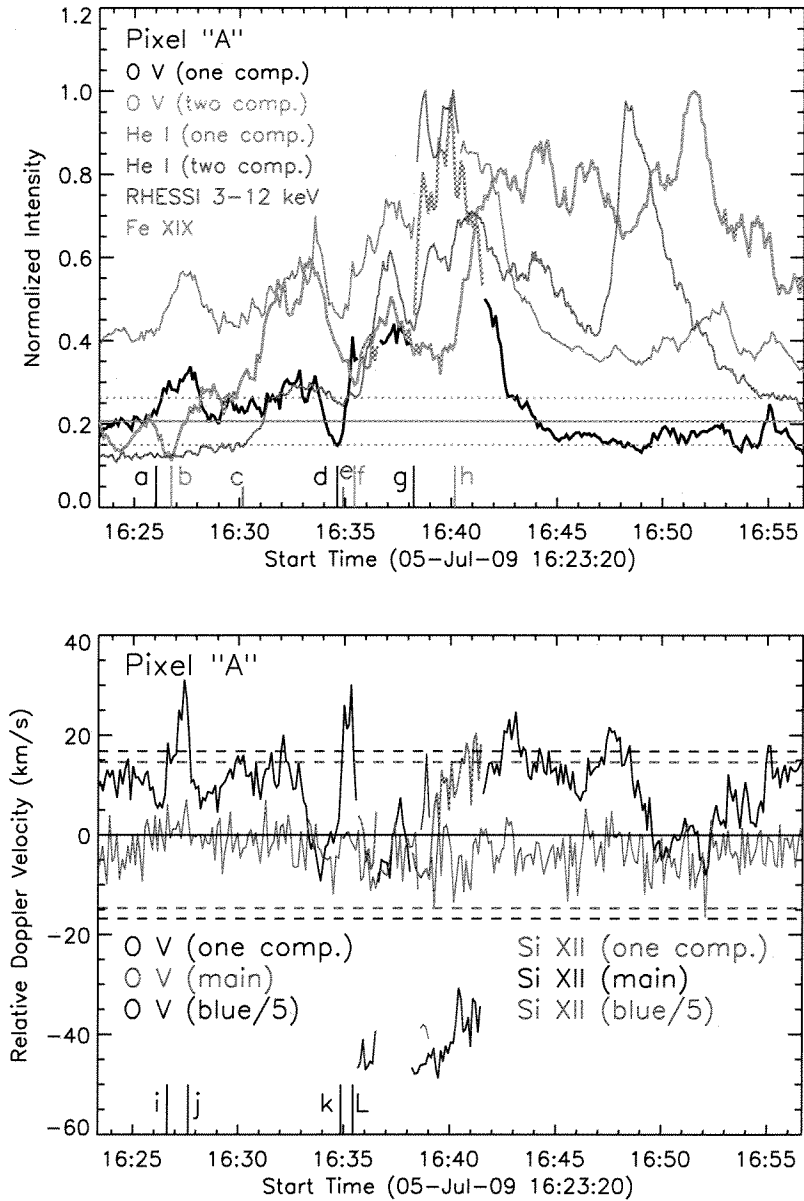
Fig. 6.— (top) Normalized (separately) He I, O V, and Fe XIX light curves in CDS pixel A, along with the normalized *RHESSI* whole Sun 3-12 keV light curve. The color scheme is indicated in the upper left. For intervals in which two components are observed, the displayed intensity is the sum of the primary and secondary components. The start times for various events are indicated with solid vertical lines on which the labels correspond to entries in Table 2. The Fe XIX intensity has been smoothed with a 9-point running boxcar. (bottom) Relative Doppler velocities measured with O V and Si XII. The color scheme is indicated toward the bottom of the frame. For exposures in which only one component is observed in the O V line profile, its velocity is plotted in black; for exposures in which two O V components are observed, the main (brightest) one is displayed in dark blue and the secondary (fainter but highly blueshifted one) is displayed in brown. The velocity of the blueshifted component is divided by 5 in order to reduce the vertical plot range.
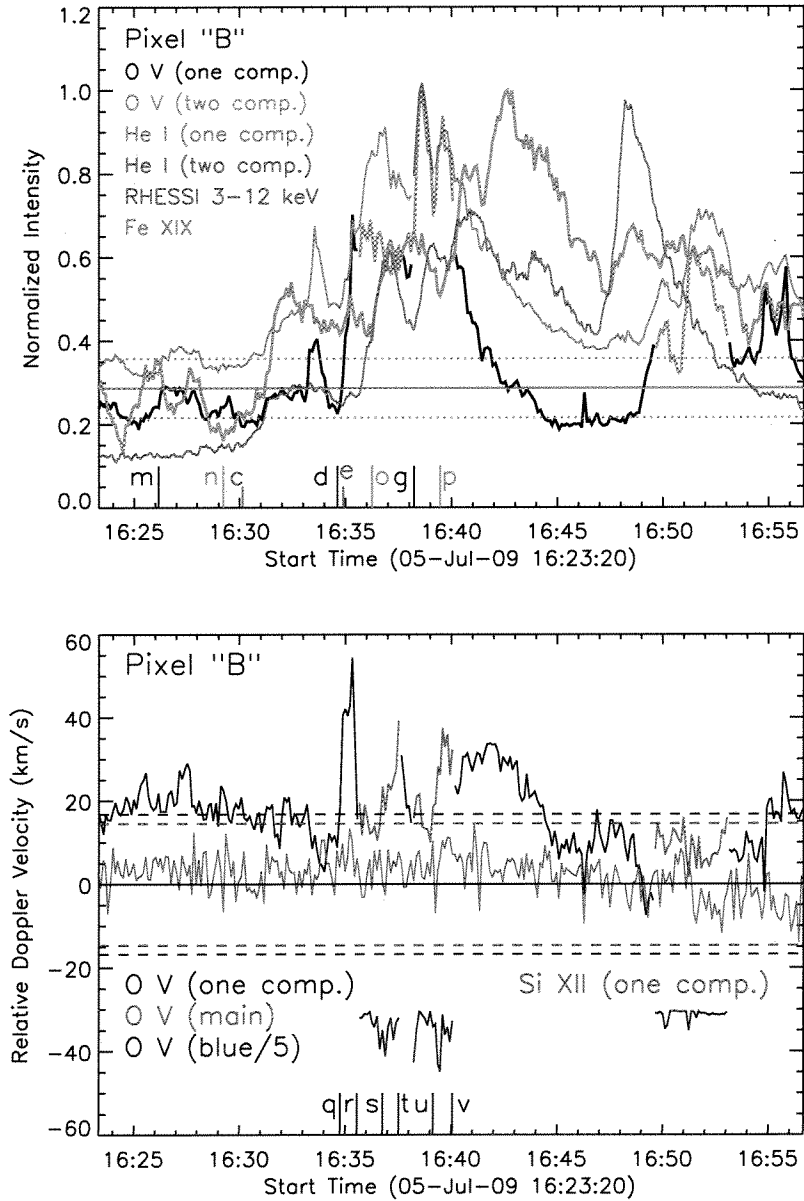
Fig. 7.— (top) Normalized (separately) He I, O V, and Fe XIX light curves in CDS pixel B, along with the normalized *RHESSI* whole Sun 3-12 keV light curve. The color scheme is indicated in the upper left. For intervals in which two components are observed, the displayed intensity is the sum of the primary and secondary components. The start times for various events are indicated with solid vertical lines on which the labels correspond to entries in Table 2. The Fe XIX intensity has been smoothed with a 9-point running boxcar. (bottom) Relative Doppler velocities measured with O V and Si XII. The color scheme is indicated toward the bottom of the frame. For exposures in which only one component is observed in the O V line profile, its velocity is plotted in black; for exposures in which two O V components are observed, the main (brightest) one is displayed in dark blue and the secondary (fainter but highly blueshifted one) is displayed in brown. The velocity of the blueshifted component is divided by 5 in order to reduce the vertical plot range.